

First-principles study of the polar O-terminated ZnO surface in thermodynamic equilibrium with oxygen and hydrogen

B. Meyer

Lehrstuhl für Theoretische Chemie, Ruhr-Universität Bochum, 44780 Bochum, Germany

(Dated: October 28, 2018)

Using density-functional theory in combination with a thermodynamic formalism we calculate the relative stability of various structural models of the polar O-terminated (000 $\bar{1}$)-O surface of ZnO. Model surfaces with different concentrations of oxygen vacancies and hydrogen adatoms are considered. Assuming that the surfaces are in thermodynamic equilibrium with an O₂ and H₂ gas phase we determine a phase diagram of the lowest-energy surface structures. For a wide range of temperatures and pressures we find that hydrogen will be adsorbed at the surface, preferentially with a coverage of 1/2 monolayer. At high temperatures and low pressures the hydrogen can be removed and a structure with 1/4 of the surface oxygen atoms missing becomes the most stable one. The clean, defect-free surface can only exist in an oxygen-rich environment with a very low hydrogen partial pressure. However, since we find that the dissociative adsorption of molecular hydrogen and water (if also the Zn-terminated surface is present) is energetically very preferable, it is very unlikely that a clean, defect-free (000 $\bar{1}$)-O surface can be observed in experiment.

PACS numbers: 68.47.Gh, 68.35.Md, 68.35.Bs, 71.15.Mb, 82.65.+r

I. INTRODUCTION

To understand the structure, composition and stability of polar surfaces on a solid theoretical basis is one of the challenging problems in surface science.¹ The most interesting polar surfaces are so called “Tasker-type(3)” surfaces² which are formed by alternating layers of oppositely charged ions. Assuming a purely ionic model³ in which all ions are in their formal bulk oxidation state, such a stacking sequence creates a dipole moment perpendicular to the surfaces which diverges with slab thickness, and with simple electrostatic arguments it can be shown that the surface energy will diverge with sample size.² To quench the dipole moment and to make the polar surfaces stable, a redistribution of charges in the surface layers has to take place.⁵ For various polar surfaces different mechanisms to accomplish the charge compensation have been observed,⁶ however, in many cases the underlying stabilization mechanism is very controversially discussed in the literature.

One of the most widely investigated examples of Tasker-type(3) polar surfaces are the two basal planes of ZnO: the O-terminated (000 $\bar{1}$)-O and the Zn-terminated (0001)-Zn surface. The two surfaces are the terminating planes of a stacking sequence of hexagonal Zn and O layers along the crystallographic *c*-axis with alternating distances of $R_1=0.61$ Å and $R_2=1.99$ Å. In this case, as can be easily shown^{1,7}, the polar ZnO surfaces are only stable if the O-terminated face is less negative and the Zn-terminated surface layer less positively charged compared to the formal bulk oxidation state by a factor of $R_1/(R_1 + R_2) \approx 1/4$. In principle, three different scenarios are conceivable to accomplish this charge redistribution: The ionic charge of the surface ions may be reduced from ± 2 to $\pm 3/2$, which may be regarded as an “electron transfer” from the O- to the Zn-terminated surface (Ia). As a result, partially occupied surface bands will appear

with a 3/4 filled O- $2p$ band at the (000 $\bar{1}$)-O and a 1/4 filled Zn- $4s$ band at the (0001)-Zn surface. This is often referred to as “intrinsic surface state compensation”⁵ or as “metalization of the polar surfaces”.⁸ However, whether a true metallic state is present will depend on the dispersion of the partially occupied bands. Additionally, in a second step, the surface may reconstruct and undergo a distortion in which, for example for the O-terminated surface, four surface atoms combine in such a way that an unoccupied $2p$ -band splits from the other eleven occupied $2p$ -bands and the surface becomes insulating again (Ib). Secondly, the charge reduction of the surface layers may take place by removing 1/4 of the surface ions (II). The so created vacancies may be ordered and form a reconstruction or may be randomly distributed. Finally, charged species may be adsorbed to reduce the formal oxidation state of the surface ions (III). For example, water may dissociate and protons (H⁺) and hydroxyl groups (OH⁻) adsorb on every second O and Zn surface ion, respectively.⁹ All three scenarios represent idealizations of the charge compensation process. In general, any combinations of the three mechanisms are conceivable, like the simultaneous formation of vacancies and partially filled bands, as long as the charge compensation rule is obeyed. The surface structure finally realized for a specific polar surface will then be the one with the lowest surface energy.

For ZnO it was believed for a long time that both polar surfaces exist in an unreconstructed, truncated-bulk-like state. After standard preparation procedures both surfaces show regular (1 \times 1) pattern in low-energy electron diffraction (LEED)¹⁰ and other diffraction experiments.^{8,11,12} Some evidence for missing Zn ions on the (0001)-Zn surface was found in grazing incidence X-ray diffraction (GIXD)¹¹, however, for the (000 $\bar{1}$)-O surface no evidence for substantial amounts of surface oxygen vacancies was detected in GIXD¹¹ and

low-energy alkali-ion scattering (LEIS).¹²

For ideal, truncated-bulk-like surface terminations only mechanism (Ia) can explain the stability of the polar ZnO surfaces. Consequently, in most theoretical first-principles studies of the polar ZnO surfaces ideal surface terminations together with partially filled surface bands were assumed.^{7,8,13} Studies exploring the other two stabilizations mechanisms are very scarce. In a pioneering ab-initio study Wander and Harrison¹⁴ investigated whether the polar surfaces may be stabilized by the dissociation of water and the adsorption of H^+ and OH^- groups according to mechanism (III). They found this energetically unfavorable compared to situation (Ia). However, instead of 1/2 monolayers, which would be the ideal configurations for band filling, only full monolayers of H^+ and OH^- were considered, thereby overcompensating the needed charge transfer between the polar surfaces. In addition, only one specific adsorption site for the H^+ and OH^- groups was probed.

Meanwhile two recent experiments have created considerable doubt that the polar ZnO surfaces really exist in a clean, unreconstructed state. With scanning tunneling microscopy (STM) it was shown^{15,16} that the Zn-terminated surface is characterized by the presence of nanoscaled, triangular islands with a height of one ZnO double-layer. The shape of the islands is size-dependent and typical pit structures appear for larger islands. Since the step edges are O-terminated, the high step concentration leads to a significant decrease of Zn ions in the surface. A rough analysis of the island and pit size distribution yielded that approximately 1/4 of the Zn ions is missing, in agreement with mechanism (II). With detailed density-functional theory (DFT) calculations^{15,17} it was confirmed that a crystal termination with triangular shaped islands and pits is indeed lower in energy than the perfect bulk-truncated surface for a wide range of oxygen and hydrogen chemical potentials. Under H rich conditions, structures with up to 1/2 monolayer of hydroxyl groups were even more stable, indicating that the actual surface morphology will sensitively depend on the chemical environment.

On the other hand, for the O-terminated polar surface no such island and pit structure was found with STM.¹⁶ However, with He scattering (HAS) it was discovered¹⁸ that at ultrahigh vacuum (UHV) conditions O-terminated surfaces with (1×1) LEED and HAS diffraction pattern are always hydrogen covered, whereas after a careful removal of the hydrogen a (1×3) structure is found. The (1×3) spots are best visible in HAS, but under certain conditions can also be observed in LEED.¹⁸ The H-free surface is very reactive and dissociates molecular hydrogen and water and therefore exists only for a limited time even at UHV conditions. In a subsequent study^{19,20,21,22} CO was used as a probe molecule to distinguish between clean and hydrogen saturated surfaces. By comparing calculated CO adsorption energies for different surface structures with experimental results it was confirmed that the polar O-terminated surface is usu-

ally hydrogen covered whereas a clean (1×1) (000 $\bar{1}$)-O surface is very unlikely to exist.

In previous studies the H coverage of the polar O-terminated surface was not observed most likely because LEED and X-rays are not sensitive to hydrogen. However, it is not clear how the structures found in the HAS study, Ref. 18, lead to a stabilization of the polar O-terminated surface. A full hydrogen monolayer would overcompensate the charge transfer so that again partially occupied bands have to be present, and the nature of the H-free (1×3) structure is still unknown. There is some evidence from X-ray photoelectron spectroscopy (XPS)¹⁸ that oxygen vacancies are involved, but 1/3 of the oxygens missing is also not the expected vacancy concentration to stabilize the surface.

Motivated by these experimental findings we explore in the present paper the competition between the three stabilization mechanisms in a very general way. The main focus will be on the O-terminated (000 $\bar{1}$)-O surface, and we take an approach very similar in spirit to the investigation of the Zn-terminated surface in Ref. 15 and 17. For a series of surface models we determine the total energies and the fully relaxed atomic structures using a first-principles DFT approach. Surface structures with various oxygen vacancy concentrations and different amounts of adsorbed hydrogen are considered, including structures corresponding to the three ideal stabilization scenarios and structures compatible with the HAS observations.

Static total-energy DFT calculations only give results for zero temperature, zero pressure and for surfaces in contact with vacuum. However, the actual lowest-energy structure of the (000 $\bar{1}$)-O surface will depend on the environment and can change with temperature T , pressure p and exposure to O_2 and H_2 gas phases. Therefore, to determine the equilibrium structure and composition of the surface at finite temperature and oxygen and hydrogen partial pressures, we combine our DFT results with a thermodynamic description of the surfaces. To take deviations in surface composition and the presence of gas phases into account, we introduce appropriate chemical potentials²³ and calculate an approximation of the Gibbs free surface energy.⁴ Depending on the chemical potentials we then determine the surface structure with the lowest free energy which allows us to construct a phase diagram for the surface. If we assume that the surface is in thermodynamic equilibrium with the gas phases, we can relate the chemical potentials to a given temperature T and pressure p . In this way we are able to extend our zero temperature and zero pressure DFT results to experimentally relevant environments, thereby bridging the gap between UHV-like conditions and temperatures and gas phase pressures that are typically applied, for example, in catalytic processes like the methanol synthesis.²⁴

II. COMPUTATIONAL APPROACH

A. Thermodynamics

In this section we will give a brief description of the thermodynamic formalism which we have used to determine the most stable structures of the polar O-terminated ZnO surface. The formalism has been successfully applied in several previous surface studies^{15,25,26,27,28,29} and is described in more detail in Refs. 4 and 29.

The general expression for the free energy of a surface in equilibrium with particle reservoirs at the temperature T and pressure p is given by³⁰

$$\gamma(T, p) = \frac{1}{A} \left(G(T, p, \{N_i\}) - \sum_i N_i \mu_i(T, p) \right), \quad (1)$$

where $G(T, p, \{N_i\})$ is the Gibbs free energy of the solid with the surface of interest, A is the surface area, and μ_i , N_i are the chemical potentials and particle numbers of the various species. In contrast to the usual convention in macroscopic thermodynamics we define here the chemical potentials per atom rather than per mole. For the study of the polar O-terminated ZnO surface in contact with an oxygen and a hydrogen gas phase we have to consider the three chemical species $i = \text{Zn, O and H}$.

For simplicity we have assumed two independent reservoirs for O_2 and H_2 with a common pressure p . Experimentally, it is more likely that a mixture of O_2 and H_2 is present. In this case, the pressure p in Eq. (1) has to be replaced by appropriate partial pressures p_{O_2} and p_{H_2} . However, in the present study we will keep the restriction of separate reservoirs in the sense that we do not allow O_2 and H_2 to react to H_2O , which would be the case in full thermodynamic equilibrium. This is justified by arguing that the reaction barrier for the formation of H_2O is high enough that the reaction plays no role on the time scales of interest.

In thermodynamic equilibrium the chemical potentials would be determined uniquely by the temperature T , the pressure p and the total particle numbers of the solid and the gas phases. The surface structure, here represented by the particle numbers N_i , would then be determined by an unconstrained minimization of the surface free energy, Eq. (1). However, this is not very practical to do. Therefore we will take a different approach: We calculate the surface free energy of a series of model surfaces with different structures and compositions as a function of the chemical potentials. For given chemical potentials we predict which surface structure is the most stable one by searching for the surface model with the lowest surface free energy. In a second step, the chemical potentials are then related to actual temperature and pressure conditions by assuming that the surface is in thermodynamic equilibrium with the gas phases.

In our calculations all surfaces are represented by periodically repeated slabs so that the Gibbs free energy

$G(T, p, \{N_i\})$ refers to the content of one supercell. Since ZnO is not centrosymmetric, slabs representing the polar ZnO surfaces are inevitably O-terminated on one side and Zn-terminated on the other side. It is therefore not possible to assign unique surface energies to the two polar surface terminations. Only the sum of the surface energies and thereby the cleavage energy are well defined quantities. However, in the present study we are only interested in the *relative* stability of O-terminated surfaces with different structures and compositions. The Zn-face of the slabs is unchanged in all calculations. Therefore we relate all energies relative to a reference state which we have taken to be the ideal, truncated-bulk termination. We define the change of the cleavage energy $\Delta\gamma$ as the difference of Eq. (1) for a slab with a chosen surface structure and a slab with ideal surface terminations:

$$\Delta\gamma(T, p) = \frac{1}{A} \left(G_{\text{slab}}^{\text{surf}}(T, p, N_V, N_H) - G_{\text{slab}}^{\text{ref}}(T, p) + N_V \mu_{\text{O}}(T, p) - N_H \mu_{\text{H}}(T, p) \right). \quad (2)$$

Here, $G_{\text{slab}}^{\text{surf}}$ and $G_{\text{slab}}^{\text{ref}}$ are the Gibbs free energies of the supercells with the model surface and the reference configuration, respectively, and A is now the area of the surface unit cell. Since we only consider structures of the O-terminated surface with O-vacancies and adsorbed H atoms, only the number of O-vacancies N_V (= difference of the number of O-atoms in the slab with the model surface and the reference state) and the number of adsorbed H atoms N_H appears in Eq. (2), i.e. the chemical potential of Zn drops out. The difference $\Delta\gamma$ is negative if a model surface is more stable than the ideal, truncated-bulk-like surface termination and positive otherwise.

In principle we now have to calculate the Gibbs free energy of all slabs representing our surface models, including the contributions coming from changes in volume and in entropy. The entropy term may be calculated, for example, by evaluating the vibrational spectra in a quasiharmonic approximation³¹, but in practice this is computationally very demanding. As is apparent from Eq. (2), only the *difference* of the Gibbs free energy of two surface structures enters the expression for $\Delta\gamma$. In Ref. 29 it was shown that the vibrational contributions to the entropy usually cancel to a large extent and that the influence of volume changes are even smaller. Therefore we will neglect all entropy and volume effects. The Gibbs free energies then reduce to the internal energies of the slabs and we can replace $G_{\text{slab}}^{\text{surf}}$ and $G_{\text{slab}}^{\text{ref}}$ in Eq. (2) by the energies as directly obtained from total-energy (e.g. DFT) calculations.

Finally we have to determine meaningful ranges in which we can vary the chemical potentials. First, there are upper bounds for all three chemical potentials μ_{O} , μ_{H} and μ_{Zn} , beyond which molecular oxygen and molecular hydrogen would condensate and metallic Zn would crystallize at the surface. These bounds are given by the total energy of the isolated molecules E_{O_2} , E_{H_2} and of

bulk Zn $E_{\text{Zn}}^{\text{bulk}}$ (neglecting volume and entropy effects):

$$\mu_{\text{O}} \leq \frac{1}{2}E_{\text{O}_2}, \quad \mu_{\text{H}} \leq \frac{1}{2}E_{\text{H}_2}, \quad \mu_{\text{Zn}} \leq E_{\text{Zn}}^{\text{bulk}}. \quad (3)$$

In the following we will use these upper bounds as zero point of energy and relate the chemical potentials relative to the total energies of the isolated molecules:

$$\Delta\mu_{\text{O}} = \mu_{\text{O}} - \frac{1}{2}E_{\text{O}_2}, \quad \Delta\mu_{\text{H}} = \mu_{\text{H}} - \frac{1}{2}E_{\text{H}_2}. \quad (4)$$

Furthermore we impose that the surface is always in equilibrium with the ZnO bulk phase. Then the sum of μ_{O} and μ_{Zn} has to be equal to the total energy E_{ZnO} of bulk ZnO. Thus only one of the two chemical potentials μ_{O} and μ_{Zn} is independent, and together with Eq. (3) we introduce lower bounds for the chemical potentials. Using the energy of formation E_{f} of ZnO:

$$E_{\text{f}} = E_{\text{ZnO}} - E_{\text{Zn}} - \frac{1}{2}E_{\text{O}_2} \quad (5)$$

the allowed range for the chemical potential $\Delta\mu_{\text{O}}$ is given by:

$$E_{\text{f}} \leq \Delta\mu_{\text{O}} \leq 0. \quad (6)$$

If we assume that the surfaces are in thermodynamic equilibrium with the gas phases we can relate the chemical potentials $\Delta\mu_{\text{O}}$ and $\Delta\mu_{\text{H}}$ to a given temperature T and partial pressures p_{O_2} and p_{H_2} . For ideal gases we can use the well-known thermodynamic expressions²⁹

$$\Delta\mu_{\text{O}}(T, p_{\text{O}_2}) = \frac{1}{2} \left(\tilde{\mu}_{\text{O}_2}(T, p^0) + k_{\text{B}}T \ln(p_{\text{O}_2}/p^0) \right) \quad (7)$$

and

$$\Delta\mu_{\text{H}}(T, p_{\text{H}_2}) = \frac{1}{2} \left(\tilde{\mu}_{\text{H}_2}(T, p^0) + k_{\text{B}}T \ln(p_{\text{H}_2}/p^0) \right) \quad (8)$$

in which p^0 is the pressure of a reference state and the temperature dependence of the chemical potentials $\tilde{\mu}_{\text{O}_2}(T, p^0)$ and $\tilde{\mu}_{\text{H}_2}(T, p^0)$ is tabulated in thermochemical reference tables.³² However, it should be noted, as pointed out by Finnis³³, that the equilibrium with the gas phase need not to be perfect. It is sufficient if the surface is in equilibrium with the bulk phase. In this case, the chemical potential is related to defect concentrations of the bulk. For example, if oxygen vacancies are the dominant defects we have^{34,35,36}

$$\Delta\mu_{\text{O}}(T, p) = \tilde{\mu}_0 - k_{\text{B}}T \ln(c_{\text{V}}/c_0) \quad (9)$$

with the vacancy concentration c_{V} and the oxygen occupancy of the O-lattice site of c_0 .

B. Ab-Initio Calculations

The total energies of slabs representing different model surfaces as well as the bulk and molecular reference energies were calculated within the framework of density-functional theory (DFT).³⁷ Exchange and correlation effects were included in the generalized-gradient approximation (GGA) using the functional of Perdew, Becke and

	H ₂	O ₂	Bulk Zn	Bulk ZnO
$E_{\text{f}}^{\text{PBE}}$ [eV]	4.50	6.38	1.12	2.84
$H_{\text{f}}^{\text{exp}}$ [eV]	4.52	5.17	1.35	3.50

TABLE I: Calculated binding energies $E_{\text{f}}^{\text{PBE}}$ for the isolated H₂ and O₂ molecules and for the bulk phases of Zn and ZnO. Zero-point vibrations are not included. The experimental heat of formations $H_{\text{f}}^{\text{exp}}$ are for $T=298$ K and $p=1$ bar and are taken from Ref. 44.

Ernzerhof (PBE).³⁸ Normconserving pseudopotentials³⁹ were employed together with a mixed-basis set consisting of plane waves and non-overlapping localized orbitals for the O-2*p* and the Zn-3*d* electrons.⁴⁰ A plane-wave cut-off energy of 20 Ry was sufficient to get well converged results. Monkhorst-Pack k-point meshes⁴¹ with a density of at least (6×6×6) points in the primitive ZnO unit cell were chosen. A dipole correction^{42,43} to the electrostatic potential was included in the calculations to eliminate all artificial interactions between the periodically repeated supercells due to the dipole moment of the slabs. For more details on convergence parameters, the construction of appropriate supercell as well as the calculated bulk and clean surface structures of ZnO we refer to Ref. 7, where the same computational settings as in the present study were used.

All surfaces were modeled by periodically repeated slabs. Very thick slabs consisting of 8 Zn-O double-layers were used to reduce the residual internal electric field.⁷ To represent different surface structures (1×2), (1×3) and (2×2) surface unit cells with different combinations of O vacancies and H adatoms were considered. All atomic configurations were fully relaxed by minimizing the atomic forces.

In Table I we compare the computed binding energies of different bulk and molecular reference structures with experimental heat of formations. While the calculated binding energies for isolated H₂ molecules and bulk Zn agree quite well with experiment, there is a noticeable error of 1.2 eV in the binding energy of the free O₂ molecule. This is a well known deficiency of DFT.^{28,29} The overestimation of the O₂ binding energy is also reflected in a formation energy for ZnO which is too low by 0.6 eV. Such deviations would seriously influence our analysis of the surface energies, Eq. (2), and would alter the allowed range for the oxygen chemical potential, Eq. (6). Therefore, to circumvent errors introduced by a poor description of the O₂ molecule, we have applied the following procedure: we take the experimental value for the formation energy E_{f} of ZnO from Table I and we use Eq. (5) to replace the total energy of O₂ by E_{f} and the total energies of Zn and ZnO. E_{Zn} and E_{ZnO} are both bulk quantities which are typically more accurately described in DFT than molecular energies.

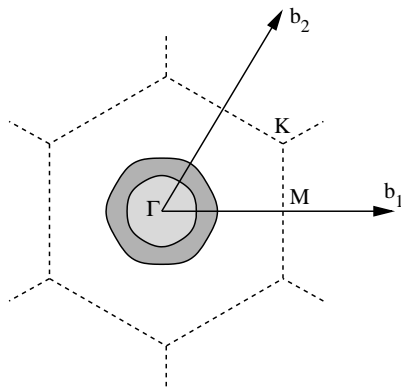


FIG. 1: Contour of the Fermi energy level for the partially occupied $(000\bar{1})$ -O surface bands plotted within the surface Brillouin zone (shown to scale). Two O- $2p$ -bands cross the Fermi level (thick solid lines). The unoccupied regions of the two bands are indicated by light gray and dark gray areas, respectively, \mathbf{b}_1 and \mathbf{b}_2 are the reciprocal lattice vectors, and the surface Brillouin zone is shown by dashed lines.

III. RESULTS AND DISCUSSION

A. Surface Distortions

First we explore the possibility whether the ideal, truncated-bulk-like $(000\bar{1})$ -O surface may lower its energy by breaking the symmetry of the surface layers, thereby adopting a distorted surface structure according to mechanism (Ib). A tendency for symmetry breaking reconstructions is often indicated by a strong nesting of the Fermi surface. In Fig. 1 we have plotted the two-dimensional Fermi surface formed by the partially occupied O- $2p$ bands. The plot represents a cut through the Brillouin zone of our supercell including only k-vectors with a zero component perpendicular to the surface. Figure 1 reveals that actually two surface bands cross the Fermi level. This is well known and in full agreement with band structure plots presented in Refs. 8 and 13. The corresponding wave functions are strongly localized at the oxygen atoms of the terminating surface layers and are mainly formed by the two O- $2p$ orbitals parallel to the surface. By integrating the occupied and unoccupied areas of the Brillouin-zone we find that indeed roughly 1/2 electron per surface atom is missing to fill the two surface bands. However, both Fermi contours are almost spherical and only a weak nesting is present.

As a second test, we did several calculations in which we randomly displaced the surface atoms in the top atomic layer of our slabs and started an atomic relaxation. Different slabs with (1×2) , (1×3) and (2×2) surface unit cells were used but in all cases the surfaces relaxed back toward a symmetric structure with a 3-fold symmetry. The surface energy was always higher than in the fully symmetric state, so that no hint for a tendency toward symmetry breaking reconstructions was found.

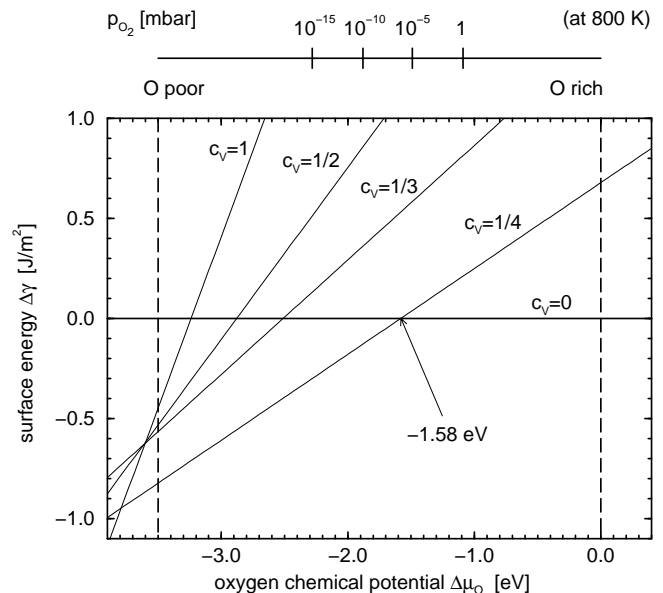


FIG. 2: Surface free energy $\Delta\gamma$ of the polar $(000\bar{1})$ -O surfaces with different concentrations of O-vacancies c_v as function of the oxygen chemical potential $\Delta\mu_O$. In the top x -axis, the chemical potential $\Delta\mu_O(T, p)$ has been translated into a pressure scale for the fixed temperature of $T=800$ K. Vertical dashed lines indicate the allowed range of $\Delta\mu_O$: For higher chemical potentials O_2 will condensate on the surface and for lower values of $\Delta\mu_O$ metallic bulk Zn can form.

B. Oxygen Vacancies

In the next step we investigate whether the $(000\bar{1})$ -O surface is stabilized by creating oxygen vacancies. From slabs with (1×1) , (1×2) , (1×3) and (2×2) surface unit cells we have removed one O-atom, thereby creating vacancy concentrations c_v of 1, 1/2, 1/3 and 1/4. In Fig. 2 we have plotted the change of the surface energy $\Delta\gamma$ of the four defect structures relative to the defect-free surface as a function of the oxygen chemical potential $\Delta\mu_O$. As to be expected from mechanism (II) the defective surface with 1/4 of the O atoms missing is the most stable surface structure over a wide range of chemical potentials. Translating the chemical potential into temperature and pressure conditions (assuming that the surface is in equilibrium with an O_2 gas phase, see upper x -axis in Fig. 2) we see that this will be the most stable surface at typical UHV-conditions of surface science experiments. However, at oxygen rich conditions (high pressure and low temperature), exceeding a chemical potential of -1.58 eV, the ideal, defect-free surface becomes the most stable structure. The other surfaces with 1, 1/2 and 1/3 vacancy concentrations are higher in energy for all chemical potentials and will therefore not be present in thermodynamic equilibrium. In particular, it is very unlikely that the (1×3) structure observed in the HAS experiment¹⁸ corresponds to a simple missing-row struc-

c_V	1	1/2	1/3	1/4 ^(a)	1/4 ^(b)
E_V [eV]	+3.24	+2.88	+2.51	+1.80	+1.58

TABLE II: Calculated vacancy formation energies E_V per O atom for removing oxygen from the ideal surface, forming O_2 molecules and a surface structure with a O vacancy concentration of c_V . (a) for a 6-fold (2×2) arrangement of the O vacancies with a separation $2a$, (b) for a rectangular O vacancy pattern with distances of $2a$ and $\sqrt{3}a$, a being the ZnO lattice constant.

ture with every third O atom removed from the surface.

At this point we should emphasize that plots like Fig. 2 strictly only allow to rule out surface structures which are higher in energy than other surface models. Since we can only perform calculations for a limited set of surface models, it is always possible that a not yet considered structure with a lower energy exists. For example, since we use periodically repeated surface unit cells of a specific size in our DFT approach, all our defect structures are perfectly ordered. It is however very well possible, that disordered or even incommensurate structures might lead to a lower energy. Additionally, there are hints that island and pit structures like the ones observed for the Zn-terminated surface¹⁵ may also for the O-terminated surface be lower in energy than the ideal surface and the surface with 1/4 vacancy concentration considered in our study.⁴⁵

In Table II we have listed O vacancy formation energies E_V which we have defined in the present context as the energy difference between the ideal surface and a vacancy surface structure of concentration c_V plus $1/2 E_{O_2}$, i.e. E_V is defined with respect to the total energy E_{O_2} of free oxygen molecules, and not, as usually done, with respect to bulk ZnO. E_V depends strongly on the vacancy concentration, indicating a strong interaction between the vacancies. Up to $c_V=1/4$ the energy cost to remove O-atoms is modest. This is not surprising since up to a vacancy concentration of 1/4 the removal of O-atoms supports the charge compensation of the O-terminated surface and will result in a better filling of the partially occupied O- $2p$ band. For higher vacancy concentrations, however, we start to overcompensate the charge transfer which stabilizes the surface. The O- $2p$ band is full now, and we have to start to fill Zn- $4s$ -states in the conduction band. Therefore the energy cost to remove more O-atoms increases rapidly.

C. Hydrogen Adsorption

We turn now to a situation in which the $(000\bar{1})$ -O surface is in equilibrium with a H_2 gas phase. H_2 molecules can dissociate, and hydrogen atoms may adsorb at the surface thereby forming OH-groups with the surface oxygen ions. Before we start to calculate the surface energy

(a) Ideal $(000\bar{1})$ -O surface:

Site:	'on-top'	'hcp-hollow'	'fcc-hollow'
ΔE [eV]	+3.16	0.0	+0.05

(b) Hydrogen covered $(000\bar{1})$ -O surface:

Site:	'on-top'	'hcp-hollow'	'fcc-hollow'
ΔE [eV]	+1.78	0.0	-0.02

TABLE III: Relative stability of the high-symmetry adsorption sites for (a) the surface O atoms of the ideal O-terminated surface and (b) the OH-groups of the H saturated surface for a full monolayer coverage. The ΔE are the calculated energy differences per O-atom/OH-group for moving the topmost O/OH-surface layer from the regular lattice position of the wurtzite structure ('hcp-hollow-site') to the 'on-top' and 'fcc-hollow' position.

for different surface models with H adatoms, we consider the possibility that the preferred adsorption site of these OH-groups is no longer the regular lattice site of the O ions. Three different high-symmetry adsorption sites are conceivable above the underlying Zn layer: an 'on-top' position, a 'hcp-hollow site', which is the regular lattice position for the O ions in the wurtzite structure, and a 'fcc-hollow site'.

First we consider the clean surface without adsorbed hydrogen. Then we see from Table III that indeed the 'hcp-hollow' sites are the most stable positions for the O surface layer. However, moving the whole layer to 'fcc-hollow' sites costs only a small amount of energy. Turning to the hydroxylated surface with a full monolayer coverage of hydrogen we find that the OH-groups now prefer the 'fcc-hollow site'. So by gradually adding hydrogen, the regular lattice site of the surface O ions becomes unstable relative to the 'fcc-hollow site'. However, the energy difference between 'fcc-' and 'hcp-hollow sites' is so small that we have neglected this effect in all further calculations and have only considered 'hcp-hollow sites' for surface oxygen atoms and OH-groups.

In the next step we construct different surface models of hydrogen covered $(000\bar{1})$ -O surfaces using a similar procedure as in Sec. III B. We take slabs with (1×1) , (1×2) , (1×3) and (2×2) surface unit cells, and we add different amounts of hydrogen to create hydrogen coverages of c_H of 1/4, 1/3, 1/2, 2/3, 3/4 and 1 monolayer.

c_H	1	3/4	2/3	1/2	1/3	1/4
E_b [eV]	-0.71	-1.10	-1.25	-1.90	-2.12	-2.20

TABLE IV: Calculated binding energies E_b per H atom for dissociating H_2 molecules and forming hydrogen layers of coverage c_H .

The calculated surface energy changes $\Delta\gamma$ relative to the clean (000 $\bar{1}$)–O surface are plotted in Fig. 3 as a function of the hydrogen chemical potential $\Delta\mu_{\text{H}}$. A very similar behavior as in Section III B arises: At H–rich conditions the structure with a 1/2 monolayer hydrogen coverage is the most stable surface, in agreement with mechanism (III). On the other hand, at H–poor conditions the clean surface without hydrogen becomes the most stable structure. As a new feature we find that between the two limiting cases the surfaces with 1/3 and 1/4 monolayer coverage are slightly more stable for small intervals of the chemical potentials.⁴⁶ Thus, by lowering the chemical potential $\Delta\mu_{\text{H}}$ from H–rich to H–poor conditions it is possible to gradually reduce the hydrogen coverage from 1/2 monolayer to 1/3, 1/4 and zero coverage. Translating the chemical potential into temperature and pressure conditions we find that we will start to remove H at UHV–pressures at a temperature of roughly 750 K, which is in reasonable agreement with the experimental observation.¹⁸ The other surface structures with hydrogen coverages larger than 1/2 are always higher in energy and will be unstable for all temperatures and hydrogen partial pressures. In particular a surface with a full monolayer of hydrogen as postulated from the results of the HAS experiment¹⁸ is not likely to exist in thermodynamic equilibrium. However, from the intensity of the He–specular peak it was deduced that only about 0.1 % of the (000 $\bar{1}$)–O surface consists of flat terraces with diameters exceeding 50 Å which contribute to the (1×1) HAS signal.¹⁸ Therefore, the H covered surface with a (1×1) HAS diffraction pattern may well be a minority phase which is formed under suitable kinetic conditions.

In Table IV we have summarized the H binding energies E_{b} per atom which we have calculated as energy difference between the ideal (000 $\bar{1}$)–O surface plus 1/2 E_{H_2} and surface structures with H coverages of c_{H} . We see that it becomes rapidly unfavorable to adsorb more hydrogen as soon as the concentration for ideal charge compensation of the polar surface of 1/2 monolayer is reached. The reason for this behavior is the same as in the case of the oxygen vacancies: Up to 1/2 monolayer of hydrogen we fill the partially occupied O–2*p*–band, beyond 1/2 monolayer the O–2*p*–band is completely filled and we have to populate the conduction band. The decrease in E_{b} from 1/2 to 1/4 monolayer coverage indicates that also at low coverages a weak repulsive interaction between the hydrogen atoms remains. This is the reason why also the low-coverage structures appear in the surface phase diagram. If we extrapolate E_{b} toward zero coverage of the surface we can estimate an initial binding energy of about 2.3 eV per H atom for the dissociative adsorption of H₂.

D. Water Dissociation

As evident from Fig. 3 hydrogen adsorption plays a major role for the stabilization of the polar (000 $\bar{1}$)–O

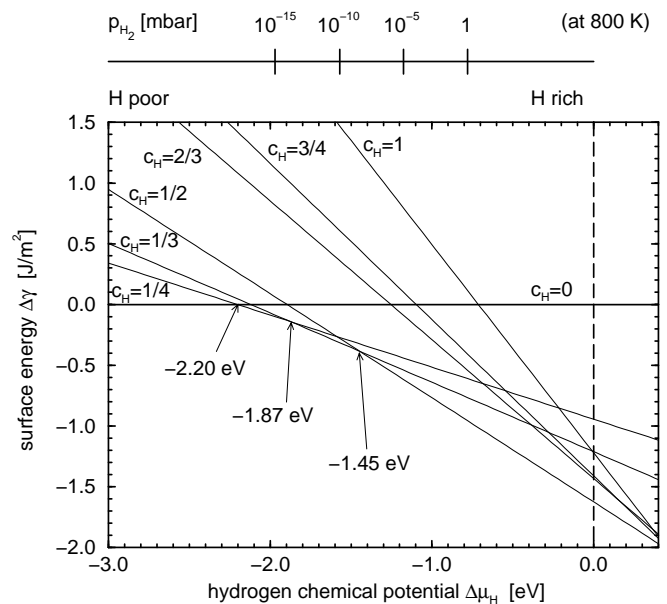


FIG. 3: Surface free energy $\Delta\gamma$ of the polar O-terminated (000 $\bar{1}$)–O surfaces with different coverages of hydrogen c_{H} as function of the hydrogen chemical potential $\Delta\mu_{\text{H}}$. In the top x -axis, the chemical potential $\Delta\mu_{\text{H}}(T, p)$ has been translated into a pressure scale for the fixed temperature of $T=800$ K. The vertical dash line indicates the upper bound for $\Delta\mu_{\text{H}}$.

surface and for almost all conceivable experimental conditions hydrogen will be present on the surface. But until now we have only considered molecular hydrogen as the reservoir for the surface hydrogen. However, in many chemical reactions and catalytic processes also water is present. Therefore we will briefly explore if also water can act as a source for surface hydrogen in the presence of the (0001)–Zn face.

In a DFT study using the hybrid B3LYP functional Wander and Harrison¹⁴ found that dissociating water and forming a full H and OH monolayer on the O– and Zn–terminated surface, respectively, is energetically unfavorable by 0.1 eV. As adsorption sites for the OH–groups they assumed the Zn ‘on-top’ positions which would be the next lattice sites for O ions if the crystal is extended. However, on the polar surfaces two more high-symmetry adsorption sites exist: the ‘hcp-hollow site’ position above atoms in the second surface layer and a ‘fcc-hollow’ site with no atoms beneath.

Using the same adsorption geometry as Wander and Harrison we also find that dissociating water is energetically unfavorable with a slightly larger energy cost of 0.3 eV. However, as shown in Table V, the configuration with the OH groups adsorbed at the ‘fcc-hollow sites’ instead of the ‘on-top’ positions is much lower in energy. Considering the correct adsorption positions for the OH groups we now find that even for the thermodynamically unstable monolayer coverages the dissociation of water is energetically preferred by about 0.4 eV. Taking only 1/2 monolayer coverages into account, this energy gain will

Site:	'on-top'	'hcp-hollow'	'fcc-hollow'
ΔE [eV]	0.0	-0.04	-0.72

TABLE V: Relative stability of the different OH adsorption sites on the polar Zn-terminated surface, calculated for a monolayer coverage.

be significantly larger.

E. Surface Phase Diagram

Finally we combine the results of the previous subsections and assume that the polar $(000\bar{1})$ -O surface is now simultaneously in equilibrium with an O_2 and a H_2 gas phase. In addition to the surface models described in Sec. III B and Sec. III C we have furthermore considered various mixed structures of O vacancies and adsorbed H atoms in the (1×2) , (1×3) and (2×2) surface unit cells.

The surface free energy now depends on two chemical potentials $\Delta\mu_O$ and $\Delta\mu_H$. The graphs of Fig. 2 and 3 therefore have to be extended to a 3-dimensional plot. Such a diagram would be rather complex and hard to follow. The most important information contained in the plot of the surface free energies is which of the surface models has the lowest surface energy for a given combination of chemical potentials $\Delta\mu_O$ and $\Delta\mu_H$. This information is better visualized if we project the 3-dimensional diagram onto the $(\Delta\mu_O, \Delta\mu_H)$ plane and only mark the regions for which a certain surface structure is the most stable one. The result is a phase diagram of the $(000\bar{1})$ -O surface which is shown in Fig. 4.

The surface phase diagram in Fig. 4 summarizes in a condensed fashion the essential results of our study. This phase diagram is dominated by two structures: a surface with 1/2 monolayer of adsorbed H and a hydrogen-free surface with 1/4 of the oxygen atoms removed. These are the two scenarios denoted as mechanism (II) and (III) in the Introduction, indicating that filling the O- $2p$ -bands is a very important mechanism to stabilize the $(000\bar{1})$ -O surface. Next to these two phases we find two structures in which H is gradually removed from the surface and only at very H-poor conditions and when plenty of oxygen is available, the ideal O-terminated surface stabilized by mechanism (I) becomes the most stable structure.

None of the additionally considered mixed structures which simultaneously contain O vacancies and H adatoms appears in the phase diagram. This is not very surprising since for the given sizes of the surface unit cells no combination of O vacancies and H adatoms exists that leads to fully occupied O- $2p$ -bands. However, it is very well conceivable that for larger surface unit cells mixed structures with, for example, an O vacancy concentration of 1/8 and a H coverage of 1/4, become more stable which would then appear as new phases between the H covered

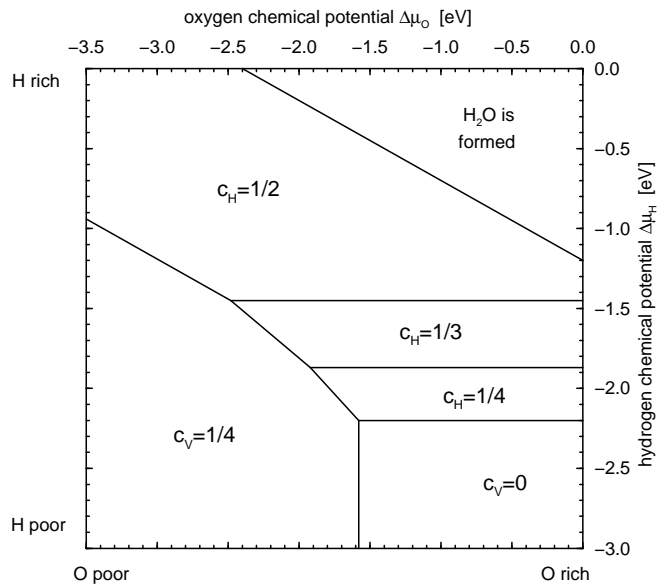


FIG. 4: Phase diagram of the polar O-terminated $(000\bar{1})$ surface in equilibrium with H and O particle reservoirs controlling the chemical potentials $\Delta\mu_H$ and $\Delta\mu_O$, based on selected superstructures as explained in the text. The lowest-energy surface structures are labeled by the concentrations of oxygen vacancies c_V and hydrogen adatoms c_H . The upper right area indicates conditions under which H_2O condensates on the surface.

and the O vacancy structures.

Relating the chemical potentials to temperature conditions and partial pressures of the gas phase shows, see Fig. 4, that for almost all realistic experimental conditions hydrogen will be present at the $(000\bar{1})$ -O surface. Even at UHV-conditions with a low hydrogen partial pressure one has to go to rather high temperatures to fully remove all hydrogen. In this case, a surface structure with O vacancies will become the most stable one. In order to stabilize the ideal O-terminated surface an oxygen atmosphere with an extremely low content of hydrogen (and also water vapor) is necessary, which is basically not achievable in experiment.

In Table VI we have summarized the surface relaxations for the three most important surface structures appearing in the surface phase diagram, Fig. 4. For the extended surface structures with H adatoms and O vacancies we have averaged in each atomic plane parallel to the surface the atomic displacements, and we define the interlayer distances d as the separation of the averaged atomic positions. Depending on the surface structure and the charge compensation process, very different surface relaxations occur. The largest relaxations are found for the clean, defect-free surface termination with a compression of the first double-layer distance of almost 50% and also a significant contraction of the second and subsequent double-layer spacings. This is in agreement with other previous ab-initio studies.^{1,7,8,13} After filling the partially occupied surface bands by adsorbing 1/2 mono-

d	ideal surface	H covered	O vacancies
H–O ₁		0.1825	
O ₁ –Zn ₂	0.0628 (–48 %)	0.1207 (0.0 %)	0.1151 (–4.6 %)
Zn ₂ –O ₃	0.3985 (+5.1 %)	0.3779 (–0.4 %)	0.3767 (–0.7 %)
O ₃ –Zn ₄	0.1077 (–11 %)	0.1246 (+3.2 %)	0.1238 (+2.6 %)
Zn ₄ –O ₅	0.3813 (+0.5 %)	0.3773 (–0.5 %)	0.3772 (–0.6 %)

TABLE VI: Summary of the averaged interlayer distances d (given in fractions of the theoretical bulk lattice constant c) and the relative changes with respect to the bulk values (in parentheses) for three different surface structures: the ideal, defect-free (000 $\bar{1}$)–O surface, the H covered surface with 1/2 monolayer of hydrogen and the surface with a vacancy concentration of 1/4. The subscripts refer to surface layers numbered from the surface plane. The theoretical PBE bulk values for the interlayer distances are $d_{\text{O–Zn}}=0.1208 c$ (in bilayer) and $d_{\text{Zn–O}}=0.3792 c$ (between bilayers) and the lattice constant was calculated to be $c=5.291 \text{ \AA}$ (see Ref. 7).

layer of H or by removing 1/4 of the O ions, however, the surface layers relax back to almost truncated-bulk-like positions. Thus, for surfaces with a lower H adatom or O vacancy concentration, surface relaxations between the two extremes are conceivable. This may explain why experimentally very different results for the surface relaxations were found. GIXD measurements^{8,11} have predicted an inward relaxation of the upper O–layer with a contraction of the first double-layer distance of 40 % and 20 %, respectively, whereas from LEED¹⁰ and LEIS¹² experiments it was concluded that the first double-layer spacing is close to its bulk value.

IV. SUMMARY AND CONCLUSIONS

By combining first-principles density-functional calculations with a thermodynamic formalism we have determined lowest-energy structures of the polar O–terminated (000 $\bar{1}$)–O surface of ZnO in thermal equilibrium with an O₂ and H₂ gas phase. This scheme allows us to extend our zero-temperature and zero-pressure DFT results to more realistic temperature and pressure conditions which are usually applied in surface science experiments or in catalytic processes like the methanol synthesis, and thus to bridge computationally the ‘pressure gap’.

The essential result of this approach is a phase diagram of the (000 $\bar{1}$)–O surface which is plotted in Fig. 4. From

this surface phase diagram we predict that hydrogen is adsorbed at the (000 $\bar{1}$)–O surface for a wide range of temperatures and H₂ partial pressures, including UHV–conditions. This is in agreement with the recent observations of a HAS experiment¹⁸ and was also confirmed in a study of the CO adsorption on the polar ZnO surfaces.¹⁹

We find a H binding energy of roughly 2.3 eV per atom if molecular hydrogen dissociates and adsorbs at the clean O–terminated surface. Furthermore we predict that in situations where both polar surface terminations are present (for example for powder samples) also the dissociative adsorption of water with H and OH–groups being adsorbed at the O– and Zn–terminated surface, respectively, is energetically preferable. However, as soon as a coverage of 1/2 monolayer of hydrogen is reached, the energy gain of adsorbing more hydrogen on the (000 $\bar{1}$)–O surface drops very rapidly with increasing hydrogen coverage. Therefore no stable phases with more than 1/2 monolayer H coverage appear in the surface phase diagram, Fig. 4. In particular, a structure with a full monolayer of H as predicted in Ref. 18 is not very likely to exist globally in thermodynamic equilibrium (which does not exclude a kinetic or local stabilization).

Going to low hydrogen partial pressures and higher temperatures it is possible to gradually remove the hydrogen from the surface and to form stable phases with less than 1/2 monolayer coverage of hydrogen. If all hydrogen is removed, oxygen vacancies will be created as was speculated in Ref. 18. However, we find that a surface with a vacancy concentration of 1/4 is much more stable than a missing-row structure where 1/3 of the oxygens has been removed. Therefore, based on the limited set of surface structures taken into consideration in our study, we currently do not understand the (1 \times 3) structure observed in Ref. 18.

Finally, at higher oxygen partial pressures the O vacancies will be filled and the clean, defect-free O–terminated surface becomes the most stable structure. However, the hydrogen partial pressure has to be very low so that we consider it very unlikely that a clean, defect-free (000 $\bar{1}$)–O surface can be observed in experiment.

V. ACKNOWLEDGMENTS

The author would like to thank Dominik Marx, Christof Wöll, Georg Kresse, and Ulrike Diebold for fruitful discussions. The work was supported by SFB 558 and FCI.

¹ C. Noguera, J. Phys.: Condens. Matter **12**, R367 (2000).

² P.W. Tasker, J. Phys. C: Solid State Phys. **12**, 4977 (1979).

³ For simplicity we use an ionic model to introduce the unfamiliar reader into the stability problem of polar surfaces.

However, the same consequences for the atomic and electronic structure of polar surfaces arise if a pure covalent bonding as in the electron-counting/auto-compensation model or a mixed ionic/covalent bonding as in the bond-

- transfer model are assumed.¹ A more general approach was given by M.W. Finnis in Ref. 4, where the polarity of a surface is related to the excess of an atomic species and the non-stoichiometry of a surface, independently of any model of the chemical bond.
- ⁴ M.W. Finnis, *phys. stat. sol. (a)* **166**, 397 (1998).
 - ⁵ R.W. Nosker, P. Mark, and J.D. Levine, *Surf. Sci.* **19**, 291 (1970).
 - ⁶ H.-J. Freund, H. Kuhlenbeck, and V. Staemmler, *Rep. Progr. Phys.* **59**, 283 (1996).
 - ⁷ B. Meyer and D. Marx, *Phys. Rev. B* **67**, 035403 (2003).
 - ⁸ A. Wander, F. Schedin, P. Steadman, A. Norris, R. McGrath, T.S. Turner, G. Thornton, and N.M. Harrison, *Phys. Rev. Lett.* **86**, 3811 (2001).
 - ⁹ In a covalent model one may argue as follows: At the polar ZnO surfaces one of the 4 nearest-neighbor bonds of the surface atoms is broken. Since O contributes 6 and Zn 2 electrons to the 4 covalent bonds, partially occupied dangling bonds will appear at the surfaces with 3/2 and 1/2 electrons per surface atom at the O- and Zn-terminated surface, respectively, forming a 3/4 and a 1/4 filled surface band. This is often referred to as “charge neutrality condition of the surface”. The partially filled bands can be avoided by a reconstruction of the surface, loss of surface atoms or by adsorption of charged species. For a more general description see Ref. 1 and 4.
 - ¹⁰ C.B. Duke and A.R. Lubinsky, *Surf. Sci.* **50**, 605 (1975).
 - ¹¹ N. Jedrecy, M. Sauvage-Simkin, and R. Pinchaux, *Appl. Surf. Sci.* **162-163**, 69 (2000); N. Jedrecy, S. Gallini, M. Sauvage-Simkin, and R. Pinchaux, *Phys. Rev. B* **64**, 085424 (2001).
 - ¹² S.H. Overbury, P.V. Radulovic, S. Thevuthasan, G.S. Herman, M.A. Henderson, and C.H.F. Peden, *Surf. Sci.* **410**, 106 (1998).
 - ¹³ J.M. Carlsson, *Comp. Mat. Sci.* **22**, 24 (2001).
 - ¹⁴ A. Wander and N.M. Harrison, *J. Chem. Phys.* **115**, 2312 (2001).
 - ¹⁵ O. Dulub, U. Diebold, and G. Kresse, *Phys. Rev. Lett.* **90**, 016102 (2003).
 - ¹⁶ O. Dulub, L.A. Boatner, and U. Diebold, *Surf. Sci.* **519**, 201 (2002).
 - ¹⁷ G. Kresse, to be published.
 - ¹⁸ M. Kunat, St. Gil Girol, Th. Becker, U. Burghaus, and Ch. Wöll, *Phys. Rev. B* **66**, 081402 (2002).
 - ¹⁹ V. Staemmler, K. Fink, B. Meyer, D. Marx, M. Kunat, S. Gil Girol, U. Burghaus, and Ch. Wöll, *Phys. Rev. Lett.*, in print.
 - ²⁰ B. Meyer and D. Marx, *J. Phys.: Condens. Matter* **15**, L89 (2003).
 - ²¹ S. Shi, C. Shi, K. Fink, and V. Staemmler, *Chem. Phys.*, (2003).
 - ²² K. Fink and A. Schwaebe, to be published.
 - ²³ G.-X. Qian, R.M. Martin, and D.J. Chadi, *Phys. Rev. B* **38**, 7649 (1988).
 - ²⁴ J.B. Hansen, *Handbook of Heterogeneous Catalysis*, G. Ertl, H. Knötzinger, J. Weitkamp (Eds.), Wiley-VCH, Weinheim, 1997.
 - ²⁵ J. Padilla and D. Vanderbilt, *Phys. Rev. B* **56**, 1625 (1997).
 - ²⁶ X.-G. Wang, W. Weiss, S.K. Shaikhutdinov, M. Ritter, M. Petersen, F. Wagner, R. Schlögl and M. Scheffler, *Phys. Rev. Lett.* **81**, 1038 (1998).
 - ²⁷ A. Pojani, F. Finocchi, and C. Noguera, *Surf. Sci.* **442**, 179 (1999).
 - ²⁸ I.G. Batyrev, A. Alavi, and M.W. Finnis *Phys. Rev. B* **62**, 4698 (2000).
 - ²⁹ K. Reuter and M. Scheffler, *Phys. Rev. B* **65**, 035406 (2001).
 - ³⁰ J.W. Cahn, in: *Interfacial Segregation*, Eds. W.C. Johnson and J.M. Blakely, American Society for Metals, Ohio (1977).
 - ³¹ W. Frank, U. Breier, C. Elsässer, and M. Fähnle, *Phys. Rev. Lett.* **77**, 518 (1996).
 - ³² D.R. Stull and H. Prophet, *JANAF Thermochemical Tables*, 2nd ed., US National Bureau of Standards, Washington DC (1971).
 - ³³ M.W. Finnis, *Psi-k Newsletter* (1999); <http://psi-k.dl.ac.uk>
 - ³⁴ J. Mayer, C. Elsässer, and M. Fähnle, *phys. stat. sol. (b)* **191**, 283 (1995).
 - ³⁵ M. Hagen and M.W. Finnis, *Phil. Mag. A* **77**, 447 (1998).
 - ³⁶ B. Meyer and M. Fähnle, *Phys. Rev. B* **59**, 6072 (1999).
 - ³⁷ P. Hohenberg and W. Kohn, *Phys. Rev.* **136**, B864 (1964); W. Kohn and L.J. Sham, *Phys. Rev.* **140**, A1133 (1965).
 - ³⁸ J.P. Perdew, K. Burke, and M. Ernzerhof, *Phys. Rev. Lett.* **77**, 3865 (1996); *Phys. Rev. Lett.* **78**, 1396 (1997).
 - ³⁹ D. Vanderbilt, *Phys. Rev. B* **32**, 8412 (1985).
 - ⁴⁰ B. Meyer, C. Elsässer, and M. Fähnle, FORTRAN 90 program for mixed-basis pseudopotential calculations for crystals, Max-Planck Institut für Metallforschung, Stuttgart.
 - ⁴¹ H.J. Monkhorst and J.D. Pack, *Phys. Rev. B* **53**, 5188 (1976).
 - ⁴² L. Bengtsson, *Phys. Rev. B* **59**, 12301 (1999).
 - ⁴³ B. Meyer and D. Vanderbilt, *Phys. Rev. B* **63**, 205426 (2001).
 - ⁴⁴ P.J. Linstrom and W.G. Mallard (Eds.), *NIST Chemistry WebBook*, NIST Standard Reference Database Number 69 (2001), National Institute of Standards and Technology, Gaithersburg MD, 20899 (<http://webbook.nist.gov>).
 - ⁴⁵ G. Kresse, private communication.
 - ⁴⁶ It might also be possible that we can gradually increase the O-vacancy concentration from zero to 1/4. However, in our calculations we did not consider surface structures with vacancy concentrations less than 1/4 so that we can not make a definite statement.